Article

Interfacial interactions as an electrochemical tool to understand Mo-based catalysts for the hydrogen evolution reaction

Nicolas Dubouis, Chunzhen Yang, Robin Beer, Lucie Ries, Damien Voiry, and Alexis Grimaud

Just Accepted

Interfacial interactions as an electrochemical tool to understand Mo-basedcatalysts for the hydrogen evolution reaction

Nicolas Dubouis,[1] Chunzhen Yang,[1] Robin Beer,[1] Lucie Ries,[2] Damien Voiry[2] and Alexis Grimaud*[1,3,4]

[1] Collège de France, 11 Place Marcelin Berthelot, 75231 Paris, France

[2] IEM, University of Montpellier, CNRS, ENSCM, Montpellier 34095, France

[3] Réseau sur le Stockage Electrochimique de l'Energie (RS2E), FR CNRS 3459, France

[4] Sorbonne Universités – UPMC Univ. Paris 06, 4 place Jussieu, F-75005 Paris, France

*corresponding author: alexis.grimaud@college-de-france.fr

Abstract

Crystalline and amorphous transition metal chalcogenides such as MoS_2 are currently recognized as state-of-the-art non-precious transition metal catalysts for the hydrogen evolution reaction (HER). Nevertheless, despite numerous studies dedicated to their electrocatalytic activities, the exact nature of the active sites as well as their interaction with interfacial water remain largely elusive. In this work, amorphous and crystalline MoS_2 catalysts were prepared by electrodeposition and chemical exfoliation respectively, and compared with other Mo-based compounds.Herein, we show thatall those compounds exhibit two reduction mechanisms in low proton concentration: the proton reduction occurring at low overpotentialfollowed by the water reduction at higher overpotential.We show that both the chemical composition and the structure of the catalyst influence the activity of the proton reduction, but that none of those materialsefficiently catalyzes the water reduction. Finally, we could demonstrate by using different cations (Li^+, Na^+ and K^+) or using deuterated electrolytes that the active sites for the proton reduction mechanism is probably different for amorphous and exfoliated crystalline MoS_2.

1

Introduction

In order to match the increasing demand for electricity storage required by the production of carbon free electricity using intermittent sources such as wind or solar energy, efficient solutions are required. Lithium-ions battery and new battery technologiessuch as Na-ions, Li-O_2, Li-S, molten salt batteries or elseare promising technologies.However they are suffering from several issues such as recyclability, safety, low energy density, etc[1,2].Dihydrogen (H_2)appears as a viable candidate as energy carrier owing from its energy density of 33,500 Wh kg^{-1}well above other carriers such as gasoline (with a theoretical energy density of 12,000Wh kg^{-1}) or other energy storage/conversion technologies such as Li-ion batteries ($\approx$400 Wh kg^{-1}).Different solutions currently exist for the production of dihydrogen, and among them water electrolysis appears as one of the most promising and cost-effective way to produce carbon-free hydrogen at large scale[3].

Nevertheless, electrochemical water splitting (2 $H_2O_{(l)}$ = 2 $H_{2(g)}$ + $O_{2(g)}$) currently suffers from large overpotentials due to the slow kinetics at the electrodes, hence requiring the use of electrocatalysts.At the anode side, transition metal oxides, such as IrO_2 or RuO_2, and oxy-hydroxides are currently consideredas the most active catalysts for the oxygen evolution reaction (OER: 2 $H_2O_{(l)}$ + 4 e^- = 4 H^+ + $O_{2(g)}$) and efforts are devoted to improve their stability and performances[4,5]. Regarding the cathode where the hydrogen evolution reaction (HER: 2 H^+ + 2 e^-= $H_{2(g)}$) takes place,platinum is currently widely recognized as state-of-the-art catalyst and used in industrial alkaline electrolyzers which led to extensivefundamental studiesthrough the use of single crystals or thin films. Nevertheless,questions still remain aboutthe electrochemical behavior of Pt with recent works pointing outtowards drastic effects of the pH on the reaction mechanism and kinetics[6–11].Despite

2

being the most active HER catalyst, the implementation of Pt into electrochemical devices suffers

from its high cost and scarcity which led to a race towards finding cost-effective and abundant HER

catalysts. Using the hydrogen adsorption as a descriptor for the HER activity, MoS_2 was proposedas a

promising catalysts based on its neither too strong nor too weak hydrogen binding[12,13].Further works

werethen carried out to identify the edges of MoS_2 grown by chemical vapor deposition (CVD) as

active sitesthanks to its low free energy barrier for proton absorption[14–16].

Following this initial demonstration of MoS_2as a potential HER catalyst, numerous works devoted to

understand the origin for this very large activity. For instance, Voiry *et al*. reported the conversion

from bulk semiconductor *2H*-MoS_2 into metallic *1T*-MoS_2nanosheets and attributed the high activity

of this material to the increased active site numbers and the improved charge transfer[17,18]whilesulfur

vacancies in the basal plane have also been considered as active sites for the HER by others[19].

Nevertheless, the different preparation methods often used for these materials make that the

determination of the HER intermediates andmechanism on those compounds still remains largely

elusive.

Aside from the works on crystalline MoS_2, a new class of HER catalysts emerged lately, namely the

amorphous andelectrodeposited MoS_x[20,21].While the initial stoichiometry for these films is of debate,

they undergo an activation step prior to HER potential so to reach an active state with a

stoichiometry close to MoS_2[21]. Recently, attempts to rationalize the HER mechanism and the activity

for amorphous MoS_x catalysts were made[22,23] but some crucial points such as the precise nature of

the active sites remain unclear.Hence, while striking similarities can be seen between these two

classes of catalysts, crystalline and amorphous chalcogenides, the lack of systematic studies hampers

drawing definitive conclusions regarding the nature of the active sites and/or the mechanism which

would allow material scientists to design better and more efficient low-cost transition metal sulfides

as HER catalysts.

Intrigued by the similarities existing between crystalline $MoS_2$and amorphous MoS_x HER catalysts, we

therefore decided to embark into a comprehensive studyfor the HER mechanism on the surface of

Mo-based catalysts. For that, we compared different Mo-based catalysts such as metallic Mo, bulk MoO_3 and MoS_2 (b-MoS_2), exfoliated 1T-MoS_2nanosheets (1T-MoS_2) and electrodeposited MoS_x film (a-MoS_x).We first demonstrate that the pH dependent HER mechanism previously reported for noble metal is ubiquitous and applies to every Mo-based catalyst,before tostudy the hydrogen adsorption on these different catalysts by examining a series of electrolytes.Doing so, we set up a new methodology to gain deeper insights into the reaction intermediates on the surface of HER catalysts.

Resultsand discussion

Comparison of MoS₂-based catalysts with other Mo-based catalysts: fromproton to water reduction

To assess the role of composition and structure on the HER performances of Mo-based catalysts, cyclic voltammetry experiments were carried out using a rotating disk electrode (RDE) in 1M H_2SO_4 solution. Results shown in Figure 1 confirm the ability of both 1T-MoS_2nanosheets and electrodeposited MoS_xfilms to efficiently reduce protons, with both catalysts exhibiting relatively low overpotentials of around 200-250 mV at 10 mA/cm²$_{geom}$. Moreover, Tafel slopes of about 45 mV per decade were found for both catalysts, in agreement with previous reports[17,20,24]. Hence, we first confirm that even if they demonstrate lower HER activity than Pt (almost no overpotential and Tafel slope as low as 26 mV per decade), both amorphous and crystalline MoS_2 perform well as HER catalysts with similar performances and metrics. On the contrary, molybdenum metal shows greater overpotential (of around 500 mV at 10 mA/cm²$_{geom}$) associated with a very large Tafel slope greater than 110 mV per decade. Interestingly, both overpotentials and Tafel slopes are reduced when bulk molybdenum oxides and sulfides are used compared to metallic molybdenum.

As a general comment, caution must be exercised when comparing the HER activity for the different catalysts. Indeed, one should note the difficulty to accurately determine the active surface area for exfoliated 1T-MoS_2 compounds as well as for MoS_x electrodeposited thin films, which could lead to

4

misevaluation of the exchange current densities. Nevertheless, this would not change the Tafel slope which is intrinsic to the material and is of prime importance for large scale application. A better understanding of the morphology of bulk materials as well asnanosheets and electrodeposited films would be required to properly compare their activity. Nevertheless, when normalized by BET surface area (Fig. S1), comparable HER activities were found for the three bulk materials at pH 0. Therefore, our experimental results suggest that the HER mechanism at low pH is very sensitive 1) to the chemical composition, with sulfides being consistently better catalysts than metal or oxides[25], and 2) to the structure of the catalyst, with nanosheets or amorphous films most likely demonstrating better performances than bulk MoS_2 when normalized by true surface area (Fig. S1).
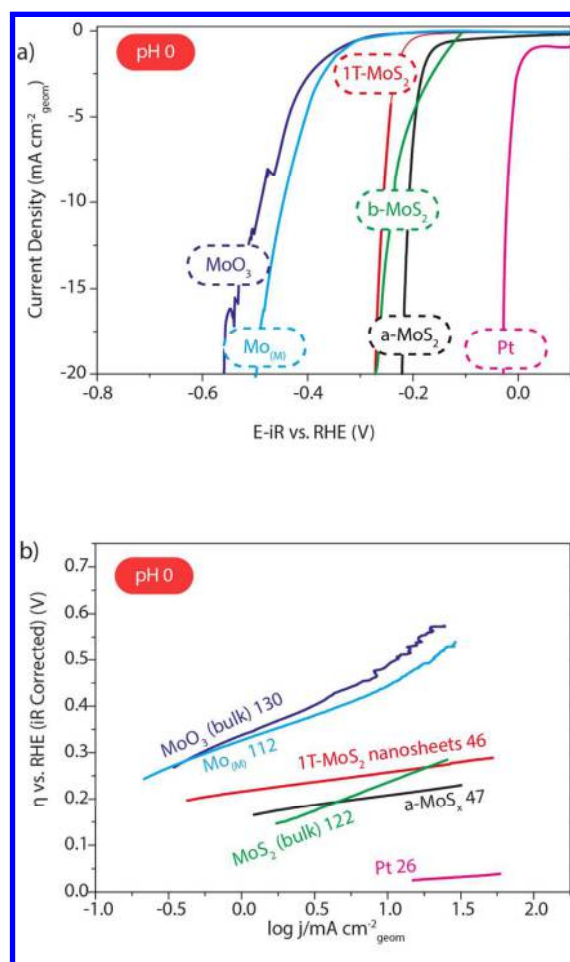
Figure 1. a) Polarization curves in 1 M H_2SO_4 (pH =0.0) in Ar at 1,600 rpm with a 20 mV s^{-1}sweeping rate and b) corresponding Tafel plots and Tafel slopes values (in mV/decade) recorded over different electrode materials. Pt referring to a polycristalline platinum electrode-(pink), a-MoS$_x$ referring to the electrodeposited MoS$_x$ films in (black), 1T-MoS$_2$ referring to the exfoliated 1T-MoS$_2$nanosheets (red), MoO$_3$ referring to commercial molybdenum oxide bulk (darkblue), b-MoS$_2$ referring to commercial MoS$_2$ bulk (green) and Mo referring to commercial Mo metal naoparticles in (light blue).

To gain deeper insights about the HER mechanism on the surface of Mo-based catalysts, electrochemical measurements were then performed at pH 4. This study is inspired by recent reports demonstrating that despite lacking any thermodynamical justification (*i.e.* the standard potential for the water reduction E°(H_2O/H_2) is expected to be the same as the one for proton reduction E°(H^+/H_2)), several HER mechanisms can occur on the surface of precious metals such as platinum,

6

gold or iridium[7,8]. Hence, while at high proton concentration the HER mechanism involves the reduction of hydronium ions ($H_3O^+ + e^- \rightarrow \frac{1}{2} H_2 + H_2O$), a second mechanism was observed when lowering the proton concentration (at pH $\geq$ 3) where the reduction/splitting of water takes place ($H_2O + e^- \rightarrow \frac{1}{2} H_2 + OH^-$)[7,8]. In contrast with the results previously obtained at lower pH (Fig. 1), the Tafel slope was found invariant and above 200 mV per decade at pH 4 for all the Mo-based catalysts (Fig. 2). Interestingly, a similar slope was obtained with Pt, which HER activity at pH 4 is also largely reduced. These results indicate that the mechanism for which water is reduced is ubiquitous to every HER catalyst, those demonstrating good performances at low pH as well as those performing poorly. These similarities between all these materials would indicate that Pt or Mo-based surfaces present no or almost no catalytic activity towards this reaction. This finding would also imply that the HER activity is, under these conditions, mainly limited by the energy necessary to break the O-H bond of the water molecule (H-O bonds in H_2O molecule are about 493 kJ mol^{-1}, compared to around 20 kJ mol^{-1} for a typical hydrogen bond). Going further into that direction, one can easily envision that once enough energy has been provided to the system so to break the O-H bond, the hydrogen adsorption (Volmer) step as well as the following step, either Tafel or Heyrovsky, would be downhill in energy. This situation drastically contrasts with the HER proceeding through hydronium reduction for which the energy of the intermediates formed on the surface of the catalyst during the reaction controls the catalytic activity, as shown by the different Tafel slopes measured for all the materials studied in this work.

Moreover, bulk Mo and MoO_3 materials tested in 1 M H_2SO_4 electrolyte suffered from a rapid decay of the HER activity over about 20 cycles, suggesting drastic dissolution or leaching processes (Fig. S2). These mechanical instabilities could be at the origin for the signal noisiness observed for these compounds upon cycling in Fig. 1. In contrary, electrodes tested at pH = 4 are activated upon cycling (Fig. S3). This activation could be the consequence of an increased in surface area by 1) increasing the porosity of the particles thanks to an electrochemical leaching or 2) modifying the morphology by exfoliation induced by the H_2 generation, as suggested recently for similar layered compounds[26]

7

.
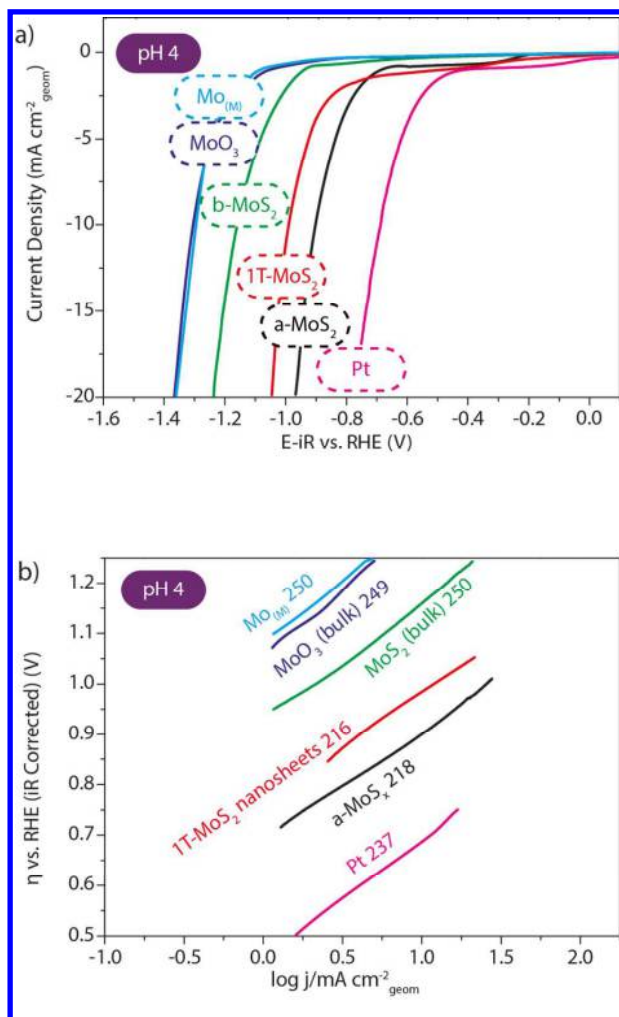
Figure 2. a) Polarization curves over different electrode materials in 0.18 mMH$_2$SO$_4$(pH =4.0) recorded in Ar at 1,600 rpm at a rate of 20 mV s^{-1} and b) corresponding Tafel plots and Tafel slopes values (in mV/decade).Ptreferring to a polycristallineplatinumelectrode (pink), a-MoS$_x$referring to the electrodeposited MoS$_x$ films in(black), 1T-MoS$_2$referring to the exfoliated 1T-MoS$_2$nanosheets(red), MoO$_3$referring to commercial molybdenum oxide bulk (darkblue), b-MoS$_2$referring to commercial MoS$_2$ bulk (green) and Mo referring to commercial Mo metal nanoparticles in (light blue).

pH dependence study for amorphous and exfoliated MoS$_2$

To further support the ubiquity of these two mechanisms, we carried out a pH dependence study for the amorphous a-MoS$_x$ and exfoliated 1T-MoS$_2$. When the proton concentration is high enough (i.e. at pH ≤ 1), the HER activity remains independent on the pH for the two compounds. This observation is consistent with a classical HER mechanism for which proton is the reactant and its reduction proceeds through twoproton-coupled electron transfer (PCET). Furthermore, Tafel slopes of around 45 mV per decade were measured for the two catalysts in this pH range, which could indicate a Volmer (H$^+$ + e$^-$ ->H$_{ads}$) / Heyrovsky (H$_{ads}$+ H$^+$ + e$^-$ -> H$_2$) mechanism, with the Heyrovsky step being the rate determining step[22]. Nevertheless, even if Tafel slopes are commonly used to identify the HER mechanism, it should be reminded that many assumptions, such as the homogeneous distribution of active sites on the surface of the catalyst, are used to calculate theoretical Tafel slopes. Special care must then be exercised, especially for the exfoliated nanosheets where active sites are reported to be concentrated on the edges of the sheets. Hence, these assumptions are probably not fulfilled and a mechanistic interpretation from Tafel slopes may not be accurate.
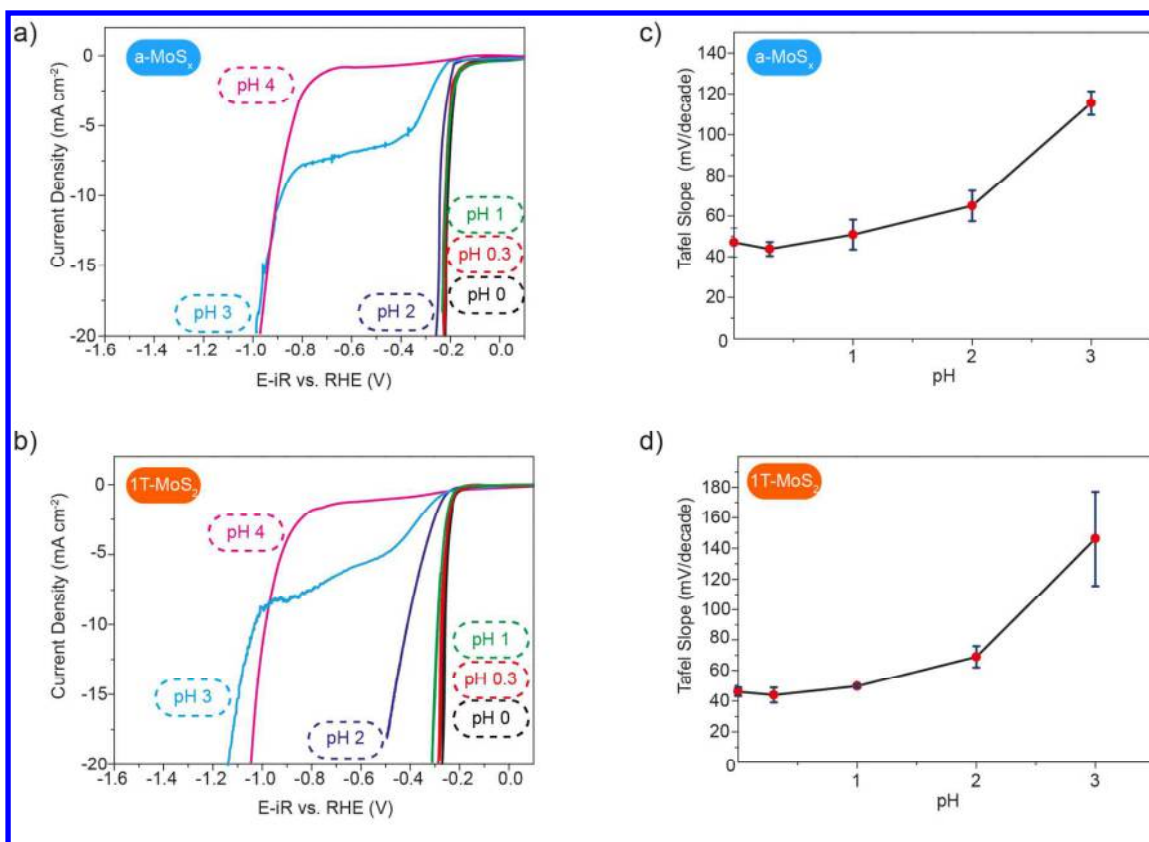
Figure 3. Polarization curves recorded at pH 0 (black), pH 0.3 (red), pH 1 (green), pH 2 (dark blue), pH 3 (light blue) and pH 4 (pink) in H_2SO_4 electrolytes over a) electrodeposited a-MoS$_x$ and b) exfoliated 1T-MoS$_2$ electrodes and corresponding Tafel slopes c) and d). Error bars were obtained by taking the deviation from the average value on three different electrodes for each pH. Different electrolytes were obtained as described in the methods part.

When increasing the pH above 1, an increase in both the overpotentials and the Tafel slopes was observed for a-MoS$_x$ and 1T-MoS$_2$. As the proton concentration is decreasing, the proton adsorption step (Volmer step) could be expected to become rate limiting. This assumption is supported by the increase of Tafel slopes at higher pH to a value close to 120 mV per decade found in the low overpotential region at pH = 3, value which would indicate the Volmer step as rate determing step. Furthermore, RDE measurements recorded at pH = 3 demonstrate for both a-MoS$_x$ and 1T-MoS$_2$ a behavior very similar to the one observed on precious metal (Pt, Ir and Au) by Strmcnik*et al*[7]. The first reduction wave at low overpotentials shows the typical exponential behavior corresponding to a

kinetically limited region and the proton reduction mechanism. A plateau can then be seen at higher

overpotential and can be attributed to the proton reduction reaction being limited by the proton

diffusion. Finally, when the overpotentialis high enough, the water reduction reaction takes place

and a typical exponential shape is once again observed. One can further notice that no diffusion

limited region can be achieved for this mechanism, owing obviously from the large concentration of

water.When further increasing the pH to 4, the proton reduction wave becomesalmost

undiscernible, and the water reduction is the main mechanism. Similar experiments were carried out

for the other materials (bulk MoO_3, bulk MoS_2, $Mo_{(M)}$, and Pt), and a similar trend was observed, as

shown in Fig S4. This study further confirms that these two different HER mechanismsare universal

and don't depend on the catalyst. This observation eventually setsa practical limitation for HER

catalysts that cannot be used at low proton concentrations. Moreover, reasonable care must be

exercise when tentatively comparing the water reduction mechanism for these compounds. Indeed,

at similar current density, noise was found for the water splitting reaction at high pH while none was

observed for the proton reduction reaction, which certainly indicates a modification of the

electrode/electrolyte interfacial area.

Looking back at thedependenceof the Tafel slopeswith pH found for a-MoS_x and 1T-MoS_2 (Fig. 3c and

3d) as well as for Pt (Fig. S5),the transition range was found independent on the materials and close

to pH 2 (slopes are found independent on the pH below this value while they increase with the pH

above this value). Thisresult excludes the surface pKa as the sole origin for this shift and further

reinforced the interpretation that two mechanisms are indeed at play.Similar observations were

made by Haghighat*et al.*who proposed, based on calculations and electrochemical

measurements,that both the reaction pathway and the mass-transfer limitation would

drasticallyimpact the electron-transfer coefficient for the Volmer step[27].

Nevertheless, under these conditions, the surface coverage of the catalysts might not be assumed

independent of the overpotential, which could also lead to Tafel slopes of 120 mV per decade even

for the Tafel-Heyrovsky mechanism, as recently discussed by Shinagawa*et al.*[22]. In order to better

11

understand the influence of pH on the proton surface coverage and a possible shift in rate determining step, numerical calculations taking into account both the electron transfer (Butler-Volmer) and mass diffusion(Levich) were conducted.

For that, Butler-Volmer equation was used to describe the rate of electrochemical steps:

$$k_i = k_i^{\circ} e^{-[\alpha_i(E - E_i^{\circ})]} \quad (1)$$

with α_i being the transfer coefficient of the electrochemical step and E_i° the standard redox potential of the electrochemical couple considered. Mass transport was then assumed to follow the Koutecký–Levich equation for RDE experiments:

$$[A]_{x=0} = [A]_{bulk} + \frac{j}{2Fm_A} \quad (2.a)$$

$$m_A = 0.620\omega^{1/2}v^{-1/6}D_A^{2/3} \quad (2.b)$$

ω being the rotation speed of the electrode, v the solvent kinematic viscosity and D_A the diffusion coefficient for the species A in the solution. Considering that the current density j can be derived from the kinetics of the rate determining step, for instance a simple electrochemical step A + e$^-$ -> A$^-$, numerical expression for j is then obtained by solving equation (3) for different values of E and the three different rate determining steps considered in this work:

$$j = \left[[A]_{bulk} + \frac{j}{2Fm_A}\right] k_{A/A^-}^{\circ} e^{-[\alpha_i(E - E_{A/A^-}^{\circ})]} \quad (3)$$

All the equations relating to the different scenarios are given in the supplementary part.

First, the surface coverage was evaluated at pH 0 for the three different scenarios: Tafel, Heyrosky and Volmer as rate determining steps (Fig. 4a). At low current density, the surface coverage was found to be almost null for every scenario, while at greater current density it is found to be independent on the potential when the Tafel step is the rate determining one. Nevertheless, under our experimental conditions (current density ≤ 20 mA/cm²), the surface coverage can be estimated as

12

very low and potential independent. As expected, a Tafel slope of about 40 mV per decade as we experimentally observed in Fig.1for both 1T–MoS$_2$ and a–MoS$_x$would indicate aVolmer-Heyrovsky mechanism, with the Heyrovsky step being the rate determining one (Fig. 4b).

Hence, to understand the increase of Tafel slope with pH previously observed, we then extended our analysis of the Heyrovsky scenario to the $0 \leq pH \leq 4$ range.When increasing the pH, a diffusion plateau for the proton reduction can be found above pH 2 (Fig. 4c). Note that the calculated current densitiesare lower than the experimental ones owing from a poor determination of the real active surface area, as we previously discussed. Interestingly, the calculated Tafel slopes were found independent on the pH for this mechanism (Fig. 4 d), unlike what was experimentally measured (Fig. 3). Thus, the large increase of the Tafel slope with the pH previously measured for all the Mo-based catalysts must originate from a change in the rate determining step, with the proton adsorption Volmer step probably being limiting above pH = 2.
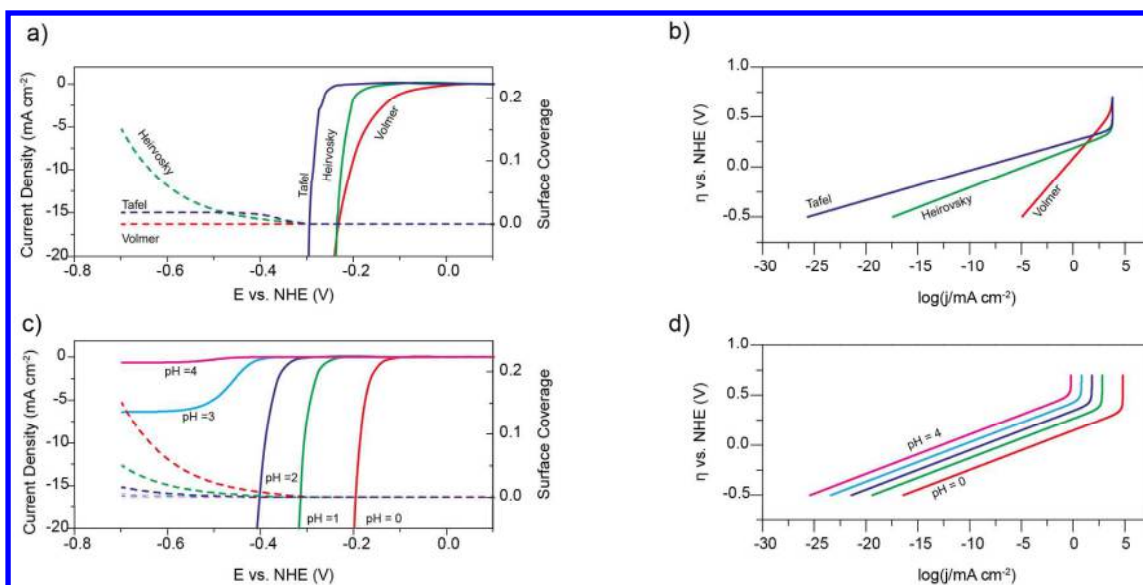
Figure 4. a) Polarization curves (solid lines) and potential dependent surface coverage (dashed lines) for different mechanism calculated using Butler-Volmer and Levich equations according to the rate determining step : Volmer (red), Heyrovsky (green) or Tafel (blue), b) corresponding Tafel plot, c) polarization curves (solid lines) and potential dependent surface coverage (dashed lines) considering the Heyrovsky step as rate determining for several pH values from 0 to 4 and d) corresponding Tafel plots. Those calculated curveswere obtained considering same conditions as in the experimental part (rotation 1,600 rpm).

Electrochemical differentiation of active sites

At that stage of the study, differences that might exist between exfoliated 1T-MoS_2nanosheets and amorphous MoS_x remain elusive. In order to get deeper insights into these inherent differences, we took advantage of the proton diffusion region observed at pH 3 which can be very sensitive to the nature of interfacial water and therefore to the electrolyte composition.Indeed,at this pH value,cations from the supporting electrolyte are in large excess (200 mM) compared to hydronium ions (1.0 mM). An effect of the supporting electrolyte can then be expected, as it has already been discussed by several groups for Pt[6,7,22], and reveal useful information about the catalysts. RDE experiments were performed using Li_2SO_4, Na_2SO_4 and K_2SO_4 as supporting electrolytes at pH 3 on a-

MoS$_x$, 1T-MoS$_2$ and platinum electrodes. As shown in Fig. S6 and Fig.S7, no significant differences can be noticed for the proton reductionreaction or for the water reduction reaction for the three different materials as a function of the supporting electrolyte under rotation. This would indicate that mass diffusion from the bulk of the electrolyteto the surface of the electrode is either not drastically modified by the cations or not controlling the reactions.
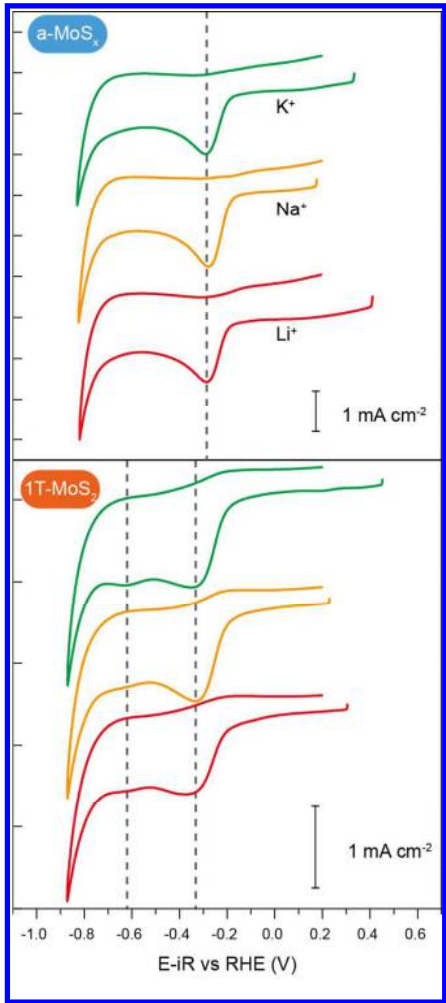
Figure 5. Static cyclovoltamograms obtained over electrodeposited a-MoS$_x$(top) and exfoliated 1T-MoS$_2$ (bottom) in several close to pH 3 electrolytes obtained by mixing 1.8 mM H$_2$SO$_4$ and 98.2 mM A$_2$SO$_4$, A being respectively Li$^+$ (red), Na$^+$ (yellow) and K$^+$ (green). A 100 mV s^{-1} sweeping rate was used For a better readability two different y-axis scales are used, each tick corresponding to 1 mA cm^{-2}.

However,under steady conditions, i.e. with no rotation, CV measurements reveal significant

15

differences between a-MoS$_x$and 1T-MoS$_2$. As shown in Figure5, the nature of the supporting electrolyte does not modify the electrochemical behavior for a-MoS$_x$which exhibits only one reduction peak at around -0.3 V vs. RHE that can reasonably be attributed to the proton reduction. This result suggests that the Gibbs free energy of formation (ΔG_{*H}) of the reaction intermediate *His not modified for the different cations. Unlike a-MoS$_x$, the electrochemical behavior for 1T-MoS$_2$was found dependent on the cation. Hence, two reduction peaks before the water splittingregion below -0.8 V can be found for K$^+$, while the second peak at higher overpotential (-0.6 V vs. RHE) almost vanished for Li$^+$ and Na$^+$. Those two peaks arelikely related to two different proton reduction reaction pathways, corresponding to the presence of two different reaction intermediates for the HER. Hence,two different types of active sitesor two different mechanisms for the same active sites must co-existfor1T-MoS$_2$, unlike a-MoS$_x$for which all active sites presumably undergo the same reaction pathway. We could be tempted to attribute the first reduction peak to the proton reduction by the most active sites located on the edges of 1T-MoS$_2$, while the second one could be related to less active sites located in the basal planes as suggested by recent reports[28].Several relevant parameters are usually discussed for the influence of cations on electrocatalysts properties such as the solvation strength or the modification of the hydrogen bonds network[6]. In light of previousX-ray diffraction (XRD) and solid-state nuclear magnetic resonance (ssNMR) reports for which thewater environment in intercalated restacked 1T-MoS$_2$nanosheets was studied[29,30],one can tentatively explain our observations. Hence, these studies reveal that water molecules are differently coordinated around the different cations: in presence of Li$^+$ or Na$^+$, 6 water molecules are solvating the cation while only two are solvating K$^+$. We could therefore explain our results by the very high sensitivity of the less active site for 1T-MoS$_2$ on the structure of the interfacial water.We then performed the same experiments on platinum electrodes for whichonly one reduction peak independent on the nature of the supporting electrolyte can be seen (Fig. S9). This result therefore corroborates the existence of a single type of active site for a-MoS$_2$. Finally, the shift of about 50 mV in the reduction peak observed between a-MoS$_x$(-0.28 V vs. RHE) and 1T-MoS$_2$(-0.32/-0.34 V vs. RHE depending on the cation)

16

indicates different energy for the *H intermediate of the proton reduction reaction for these two

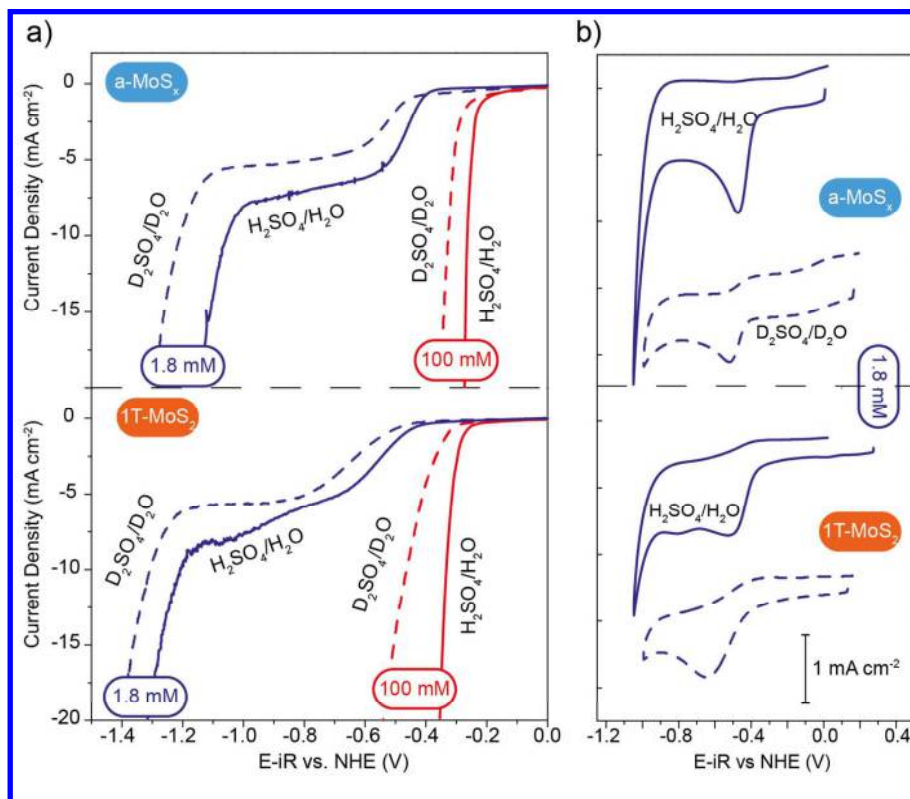catalysts, which suggests differences between the active sites.

Figure6. a) Polarization curves recorded in normal (solid lines) or deuterated electrolytes (dashed lines) 100 mM acid (red) and 1.8 mM (blue) at 20 mV s^{-1} using a RDE at 1,600 rpm and b) corresponding static CVs recorded in the 1.8 mM acid electrolytes at 100 mV s^{-1}over amorphous MoS$_2$ (top) and exfoliated 1T-MoS$_2$ (bottom) electrodes. In b), each tick on the left axis corresponds to 1 mA cm^{-2}.

To clarify our observations and further understand the complexity of the interactions catalyst/interfacial water,isotopic effects were studied. For that, several D$_2$SO$_4$ in D$_2$O electrolytes were employed and electrochemical behaviors compared with those previously measured using H$_2$SO$_4$ in H$_2$O electrolytes.Unlike previous experiments, results are reported in Fig. 6vs. the normal hydrogen electrode (NHE) as pH and pD cannot be simply compared.Before any interpretations, it should be reminded that using deuterium strongly modifies the electrolyte properties, especially by decreasing the diffusion coefficient of the reactant (4.10^{-5} cm^{-2} s^{-1} for D$_3$O$^+$in D$_2$O compared to 7.10^{-}

^{5}cm^{-2} s^{-1}for H$_3$O$^+$in H$_2$O[31]) as well as shifting the standard potential for the reaction (E°(D$^+$/D$_2$) ≈-6 mVvsRHE[32,33]).While no drastic modifications were found for Pt when comparing D$_2$O and H$_2$O measurements (as shown in Fig. S8), a large shift to greater overpotential is observed for a-MoS$_x$ and 1T-MoS$_2$ when using D$_2$O solutions. Regarding a-MoS$_x$, limitations related to proton diffusion within the porosity of the film could explain this shift.Nevertheless, since 1T-MoS$_2$catalyst is dense, the shift must originate from other limitations. Tafel slopes were then calculated for both compounds in the 100 mMH$_2$SO$_4$/D$_2$SO$_4$electrolytes. Hence the slope measured for a-MoS$_x$in the deuterated electrolyte (46±5 mV/decade) is similar to the slope obtainedinH$_2$O electrolyte (50±7 mV/decade), which advocates for limitations related to diffusion within the film. However, for 1T-MoS$_2$ the Tafel slope significantly increaseswhen using deuterated electrolyte (50 ±2 mV/decade in H$_2$O and 66 ± 8 mV/decade in D$_2$O). We could be tempted to explain this observation by stronger D-D bond when compared to H-H bond (respectively 443 and 436 kJ mol^{-1}) which would slower the rate limiting step. Nevertheless, similar behavior should then be expected for a-MoS$_x$.Hence, the change in Tafel slopes suggests than the free enthalpy of formation of the HER intermediate for 1T-MoS$_2$is modifiedwhen using deuterium,or that the surface coverage of *D decreases, hence slowing down the rate for the D$_2$ evolution step.

When decreasing the concentration of sulfuric acid to 1.8 mM (deuterated or not)similar observations can be made. More specifically, CVs recorded without rotation highlight the fundamental differences existing between a-MoS$_x$ and 1T-MoS$_2$ (Fig. 6b). For a-MoS$_x$, a slight shift corresponding to the proton adsorption and reduction peak is observed in deuterated solvent, associated with a weaker intensity as expected from the limitations related to diffusion within the film. For 1T-MoS$_2$, not only a shift greater than 100 mV is measured for the proton reduction peak, but the second peak previously observed in Fig. 5 disappeared. Hence, from our combined isotopic and cation studies, one can conclude that the active sites are different for a-MoS$_x$ and 1T-MoS$_2$, with the active sites being very dependent on the nature of the interfacial water for 1T-MoS$_2$.

Discussion

The results presented above reveal how interfacial interactions involved in the proton reduction reaction, and more generally in electrochemical processes, govern the kinetics of these processes. As mentioned earlier in this work, the study of the HER is challenging because of its fast kinetics, especially in low pH conditions. Fortunately, as shown in Figure 7, it is possible to gain deeper insights into the catalysts operation by triggering specific interactions. In low pH conditions, as no supporting salt is added, the only interactions at play are the ones between the catalyst and the hydronium ion, partially solvated by water molecules. To reveal these interactions, deuterated electrolytes have been used. Hence, the kinetics of the HER was shown to be altered by the D^+/H^+ isotopic effect for $1T\text{-}MoS_2$, while its remains independent on this effect for other catalysts such as a-MoS_x and Pt. This strategy has the advantage to be direct and to give information about the specific interactions governing the HER on the surface of catalysts without further modifying the proton (or deuterium) concentration. Furthermore, by increasing the pH to 3 and employing different conductive salts, we could slower the HER kinetics and demonstrate the complexity of this reaction on the surface of Mo-based catalysts. It could be tempting to uniquely attribute the effects observed on $1T\text{-}MoS_2$ and the absence of effect for a-MoS_x to a specific interaction between the cation and the active site for $1T\text{-}MoS_2$, which differs from a-MoS_xas no cationic effect would be expected if the cation is not electroactive (which would result from no specific interaction between the cation and the catalyst)[34]. However, coupling this study with results obtained in deuterated electrolytes at the same D^+/H^+ concentration (i.e. pH or pD = 3), we could undoubtedly show that the complex interactions between the catalyst surface, hydronium ions and cations from the supporting electrolyte govern the HER kinetics under these conditions. Furthermore, this unique approach could also alleviate the difficulties related to the study of HER catalysts by highlighting the differences existing between the electrochemically active sites for $1T\text{-}MoS_2$ and a-MoS_x. Finally, the interactions cations-catalyst-water appear not to be critical for the water reduction reaction at pH = 4 (Figure 6,

19

right). Indeed, the energy required for breaking O-H bond in water ($\approx$ 500 kJ mol^{-1}) is greater than the one involved for weaker interactions such as hydrogen bonding.
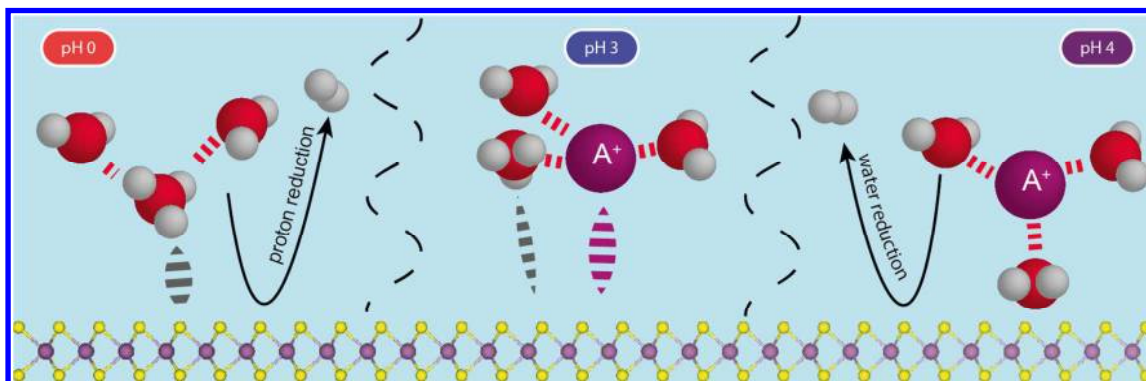

Figure 7. Schematic representation of the interactions governing the hydrogen evolution reaction kinetics on molybdenum sulfides catalysts. At pH = 0 (left), the proton reduction takes place where only hydronium interaction with the surface of the catalysts play a role. At pH = 4 (right), the water reduction reaction takes place for which interaction with cations from the supporting electrolyte does not play a critical role on the HER kinetics.Finally, at pH = 3 for which both proton reduction and water reduction reactions are in competition (center), interactions between the catalyst, water and cations from the supportingelectrolyteare essential for the HER kinetics.

Conclusion

We have demonstrated in this work the ubiquity of the two HER mechanisms on the surface of Mo-based HER catalysts: the proton reduction reaction at low pH (high proton concentration) and the water reduction reaction at high pH (low proton concentration). We could further reveal that while the proton reduction reaction is catalyzed by Mo-based catalysts, i.e. the proton adsorption energy controls the rate of the reaction, the kinetics for the water reduction reaction was found almost independent on the catalysts. This further supports previous assumptions that the kinetics for this reaction is largely dominated by the energy required to break the O-H bond in water. From this observation, we then proposed a methodology to recognize the differences existing between the active sites for amorphous MoS$_x$ films and crystalline exfoliated 1T-MoS$_2$. By varying the supporting

20

electrolyte, we found that a-MoS$_x$ shows only one active site which is largely independent on the nature of the supporting electrolyte. In contrary, two actives sites were found for 1T-MoS$_2$, with both of them being highly dependent on the nature of the interfacial water that can be modified by changing the cations in solution or replacing protons by deuterium. This work highlights the opportunity given by specific interactions to study and better understand active sites for HER catalysts, which we hope will lead to the development of better cost-effective catalysts.

Materials & methods

Materials

All chemicals (except MoS$_2$nanosheets suspension) were purchased from commercial suppliers, and used without further purification. Ultrapure Mili-Q water (18.2 MΩ·cm) was used in all experiments. Glasswares used were rinsed 3 times with ultrapure water prior to be used.

Electrodes preparation

Prior to any deposition of active material, mirror polished GC electrodes (Pine research) were polished using an ultrafine alumina slurry (0.05μm, Pine research) on a microcloth polishing disk (Pine research). As polished electrodes were sonicated in a 50:50 ethanol/water solution, two times for 15 minutes to remove Alumina particles.Same procedure was applied for the Pt disk electrode (Pine research).

a-MoS$_x$ electrodes were electrodeposited on GC electrodes by 50 consecutives CVsperformed in approximatively 5mL of a 1 mM MoS$_4$(NH$_4$)$_2$ (99.97%, Sigma-Aldrich, stored in a Ar filled glovebox) solution with a 0.1 M KCl (>99%, Alfa-Aesar) used as supporting electrolyte between -0.948 V and0.252 V vs. AgCl/Ag (3 M KCl) reference electrode. A Pt wire was used as counter electrode. CorrespondingCVs are shown in Fig. S9. The influence of the Pt counter electrode either on the deposition of a-MoS$_x$ or on the HER activity was dismissed by depositing and testing a-MoS$_x$ electrodes at pH 0 and pH 3 using a graphite rod as the counter electrode. Electrodes deposited using a Pt wire as the counter electrode did not exhibit greater performances than those deposited using a Pt wire. Also, electrodes tested using a graphite rod behaved similarly than when tested with a graphite rod (Fig S13).

1T-MoS$_2$nanosheets were prepared as described elsewhere[16].Details and characterizations (Raman spectroscopy Fig.S10 and X-Ray Photoelectron Spectroscopy Fig. S11) are given in the supplementary methods.

Molybdenum metal(3-7 μm particles, 99.95%, Alfa Aesar), MoO$_3$ (99.5%, Sigma-Aldrich), bulk MoS$_2$ (99%, Alfa Aesar) electrodes were prepared by drop-casting 10 μL of an ink on GC electrodes. The ink was prepared by mixing 20 mg of active compound, with 5 mg of active carbon in 5 mL of THF. The as prepared ink was sonicated for 30 min and then 130 μL of Nafion (5% weight in 1/1 water/1-propanol, Alfa Aesar) was added as a binder after what the ink was sonicated for 30 min.

Electrochemical measurements

Test at pH 0 and pH dependence study were conducted in H$_2$SO$_4$ electrolytes prepared from 96% sulfuric acid (Sigma-Aldrich, Sial). For electrolytes containing less than 100 mM of H$_2$SO$_4$, a supporting electrolyte was used to limit the ohmic drop. These electrolytes were prepared by mixing a 100 mM H$_2$SO$_4$ solution with a 100 mM supporting electrolyte. For instance, to obtain the pH 2 electrolyte, 18 mL of 100 mM H$_2$SO$_4$ was mixed with 100 mM K$_2$SO$_4$ electrolyte to get a final volume of 100 mL.pH 3 and pH 4 electrolytes were obtained using respectively 1.8 mM and 0.18 mM H$_2$SO$_4$ concentrations.K$_2$SO$_4$ (>99%, Alfa-Aesar) was used for all the tests, unless for cation dependence study for which Li$_2$SO$_4$ (99%, monohydrate, Alfa-Aesar), Na$_2$SO$_4$ (>99%, anhydrous, Alfa-Aesar) were used. Deuterated electrolytes were prepared the same way except that water was replaced by D$_2$O (Sigma-Aldrich, 99% D) and sulfuric acid by D$_2$SO$_4$ (Sigma Aldrich, 99.5% D).

Electrolytes were degassed in order to eliminate CO$_2$ and O$_2$by bubbling Ar (Linde, purity 5.0) for at least 30 min before first experiment and for a smaller time between different experiments. pH values of electrolytes were measured and checked by measuring the voltage E between the RHE electrode and a calomel saturated reference electrode, for which the potential was considered to be 240 mV, pH is then given by the following equation $pH = (E - 0.240)/0.059$ derived from Nernst equation.

All the electrodes were "activated" by being cycled at least 1 cycle until the current density reaches 20 mA/cm^2. Polarization curves were recorded on fresh electrodes to probe each time a clean surface(typically second cycle for a-MoS$_x$and 1T-MoS$_2$, first for Pt andMoS$_2$ bulk, MoO$_3$ and Mo$_{(M)}$, except when stability test where performed). As described in the literature, the as deposited a-MoS$_x$ undergoes a reduction which is assumed to be MoS$_{2+x}$ -> MoS$_2$ in the first cycle[21], as shown in Fig. S12.

Data were acquired using a Biologic VSP potentiostat. Ohmic drop compensation was measured using impedance spectroscopy after electrochemical measurements, and corrected during the data treatment. Typical values ranged from around 3-5 Ohms in pH = 0 electrolytes to about 35 Ohms in pH 4 electrolytes.

Supporting Information.

Details about the numerical model, supplementary electrochemical measurements and characterization for the 1T-MoS$_2$material.

Acknowledgement.

References

(1)   Bruce, P. G.; Freunberger, S. A.; Hardwick, L. J.; Tarascon, J.-M. *Nat. Mater.***2012**, *11*, 19–29.

(2)   Licht, S.; Cui, B.; Stuart, J.; Wang, B.; Lau, J. *Energy Environ. Sci.***2013**, *6* , 3646–3657.

(3)   Midilli, A.; Ay, M.; Dincer, I.; Rosen, M. A. *Renew. Sustain. Energy Rev.***2005**, *9* , 255–271.

(4)   Dau, H.; Limberg, C.; Reier, T.; Risch, M.; Roggan, S.; Strasser, P. *ChemCatChem***2010**, *2*, 724–

        761.

(5)   Hong, W. T.; Risch, M.; Stoerzinger, K. A.; Grimaud, A.; Suntivich, J.; Shao-Horn, Y. *Energy*

        *Environ. Sci.***2015**, *8*, 1404–1427.

(6)   Subbaraman, R.; Tripkovic, D.; Strmcnik, D.; Chang, K.-C.; Uchimura, M.; Paulikas, A. P.;

        Stamenkovic, V.; Markovic, N. M. *Science***2011**, *334*, 1256–1260.

(7)   Strmcnik, D.; Uchimura, M.; Wang, C.; Subbaraman, R.; Danilovic, N.; van der Vliet, D.;

        Paulikas, A. P.; Stamenkovic, V. R.; Markovic, N. M. *Nat. Chem.***2013**, *5*, 300–306.

(8)   Stamenkovic, V. R.; Strmcnik, D.; Lopes, P. P.; Markovic, N. M. *Nat. Mater.***2016**, *16*, 57–69.

(9)   Durst, J.; Siebel, A.; Simon, C.; Hasché, F.; Herranz, J.; Gasteiger, H. A. *Energy Environ. Sci.***2014**,

        7, 2255.

23

(10) Ledezma-Yanez, I.; Wallace, W. D. Z.; Sebastián-Pascual, P.; Climent, V.; Feliu, J. M.; Koper, M.

T. M. *Nat. Energy* **2017**, *2*, 17031.

(11) Costentin, C.; Giovanni, C. D.; Giraud, M.; Savéant, J.-M.; Tard, C. *Nat. Mater.* **2017**, *16*, 1016.

(12) Nørskov, J. K.; Bligaard, T.; Logadottir, A.; Kitchin, J. R.; Chen, J. G.; Pandelov, S.; Stimming, U.

J. Electrochem. Soc. **2005**, *152*, J23.

(13) Morales-Guio, C. G.; Stern, L.-A.; Hu, X. *Chem. Soc. Rev.* **2014**, *43*, 6555–6569.

(14) Hinnemann, B.; Moses, P. G.; Bonde, J.; Jørgensen, K. P.; Nielsen, J. H.; Horch, S.;

Chorkendorff, I.; Nørskov, J. K. *J. Am. Chem. Soc.* **2005**, *127*, 5308–5309.

(15) Jaramillo, T. F.; Jørgensen, K. P.; Bonde, J.; Nielsen, J. H.; Horch, S.; Chorkendorff, I.

Science **2007**, *317*, 100–102.

(16) Benck, J. D.; Hellstern, T. R.; Kibsgaard, J.; Chakthranont, P.; Jaramillo, T. F. *ACS Catal.* **2014**, *4*,

3957–3971.

(17) Voiry, D.; Salehi, M.; Silva, R.; Fujita, T.; Chen, M.; Asefa, T.; Shenoy, V. B.; Eda, G.; Chhowalla,

M. *Nano Lett.* **2013**, *13*, 6222–6227.

(18) Voiry, D.; Fullon, R.; Yang, J.; de Carvalho Castro e Silva, C.; Kappera, R.; Bozkurt, I.; Kaplan, D.;

Lagos, M. J.; Batson, P. E.; Gupta, G.; Mohite, A. D.; Dong, L.; Er, D.; Shenoy, V. B.; Asefa, T.;

Chhowalla, M. *Nat. Mater.* **2016**, *15*, 1003–1009.

(19) Lu, A.-Y.; Yang, X.; Tseng, C.-C.; Min, S.; Lin, S.-H.; Hsu, C.-L.; Li, H.; Idriss, H.; Kuo, J.-L.; Huang,

K.-W.; Li, L.-J. *Small* **2016**, *12*, 5530–5537.

(20) Merki, D.; Fierro, S.; Vrubel, H.; Hu, X. *Chem. Sci.* **2011**, *2*, 1262–1267.

(21) Vrubel, H.; Hu, X. *ACS Catal.* **2013**, *3*, 2002–2011.

(22) Shinagawa, T.; Garcia-Esparza, A. T.; Takanabe, K. *Sci. Rep.* **2015**, *5*, 13801.

(23) Deng, Y.; Ting, L. R. L.; Neo, P. H. L.; Zhang, Y.-J.; Peterson, A. A.; Yeo, B. S. *ACS Catal.* **2016**, *6*,

7790–7798.

(24) Tran, P. D.; Tran, T. V.; Orio, M.; Torelli, S.; Truong, Q. D.; Nayuki, K.; Sasaki, Y.; Chiam, S. Y.; Yi,

R.; Honma, I.; Barber, J.; Artero, V. *Nat. Mater.* **2016**, *15*, 640–646.

24

(25)   Grimaud, A.; Hong, W. T.; Shao-Horn, Y.; Tarascon, J.-M. *Nat. Mater.***2016**, *15*, 121–126.

(26)   Liu, Y.; Wu, J.; Hackenberg, K. P.; Zhang, J.; Wang, Y. M.; Yang, Y.; Keyshar, K.; Gu, J.; Ogitsu, T.;

Vajtai, R.; Lou, J.; Ajayan, P. M.; Wood, B. C.; Yakobson, B. I. *Nat. Energy***2017**, *6*, 2017127.

(27)   Haghighat, S.; Dawlaty, J. M. *J. Phys. Chem. C***2016**, *120*, 28489–28496.

(28)   Zhang, J.; Wu, J.; Guo, H.; Chen, W.; Yuan, J.; Martinez, U.; Gupta, G.; Mohite, A.; Ajayan, P.

M.; Lou, J. *Adv. Mater.***2017**, *29*, 1701955.

(29)   Alexiev, V.; Meyer zu Altenschildesche, H.; Prins, R.; Weber, T. *Chem. Mater.***1999**, *11*, 1742–

1746.

(30)   Acerce, M.; Voiry, D.; Chhowalla, M. *Nat. Nanotechnol.***2015**, *10*, 313–318.

(31)   Benderskij, V.A., Krivenko, A.G., & Rukin, A.N. *Khimiya Vysok. Ehnergij***1980**, *14*, 400–405.

(32)   McIntyre, J. D. E.; Peck, W. F. *J. Electrochem. Soc.***1970**, *117*, 747–751.

(33)   McIntyre, J. D. E.; Salomon, M. *J. Phys. Chem.***1968**, *72*, 2431–2434.

(34)   Herranz, J.; Durst, J.; Fabbri, E.; Patru, A.; Cheng, X.; Permyakova, A. A.; Schmidt, T. J. *Nano

Energy***2016**, *29*, 4–28.

25

FOR TABLE OF CONTENTS ONLY